International Journal of Thermophysics, Vol. 18, No. 3, 1997

Equation of State and Ideal-Gas Heat Capacity of a Gaseous Mixture of 1,1,1,2-Tetrafluoroethane, Pentafluoroethane, and Difluoromethane

J. J. Hurly,[1,2] J. W. Schmidt,[1] and K. A. Gillis[1]

Received August 15, 1996

We present the gas-phase equation of state and ideal-gas heat capacity of a ternary mixture (nominal molar concentration) of 1,1,1,2-tetrafluoroethane (35%), pentafluoroethane (30%), and difluoromethane (35%) for temperatures between 260 and 453 K and pressures between 0.05 and 7.7 MPa. These results were based on two very different measurement techniques. The first technique measured the gas density of the mixture in a Burnett apparatus from 313 to 453 K and from 0.2 to 7.7 MPa. The second technique deduced the gas density and ideal-gas heat capacity from high-accuracy speed-of-sound measurements in the mixture at temperatures between 260 and 400 K and at pressures between 0.05 and 1.0 MPa. The data from the two techniques were analyzed together to obtain an equation of state that reproduced the densities from the Burnett technique with a fractional RMS deviation of 0.038%, and it also reproduced the sound speeds with a fractional RMS deviation of 0.003%. Finally, the results are compared to a predictive model based on the properties of the pure fluids.

KEY WORDS: Burnett; CF_3CH_2F; CF_3CHF_2; CH_2F_2; difluoromethane; equation of state; gas density; heat capacity; pentafluoroethane; refrigerant; speed of sound; tetrafluoroethane; virial coefficient.

1. INTRODUCTION

The refrigeration industry has been searching for alternatives to fully halogenated chlorofluorocarbons (CFCs) for use as working fluids in refrigerators, chillers, and air-conditioners. Hydrofluorocarbons are a class

[1] Physical and Chemical Properties Division, Chemical Science and Technology Laboratory, National Institute of Standards and Technology, Gaithersburg, Maryland 20899, U.S.A.
[2] To whom correspondence should be addressed.

0195-928X/97/0500-0655$12.50/0

of compounds that are under test in both pure component and mixture forms. Several criteria are used to assess the utility of a candidate fluid for a particular application. First and foremost, the fluid's thermophysical properties must be commensurate with the intended operating conditions. However, additional constraints (e.g., toxicity, flammability, materials compatibility, etc.) severely limit the number of candidates that meet all of the selection criteria. Fluid mixtures provide more flexibility in the "design" of a working fluid to meet these requirements.

In this paper, we present the gas-phase equation of state and ideal-gas heat capacities of one such mixture with the molar composition 35.331% 1,1,1,2-tetrafluoroethane (HFC-134a), 30.062% pentafluoroethane (HFC-125), and 34.607% difluoromethane (HFC-32). The measurements included temperatures (T) between 260 and 453 K and pressures (P) between 0.05 and 7.7 MPa. This ternary fluid was examined with two independent experimental techniques. A Burnett apparatus directly measured the density $\rho(T, P)$ of the mixture over the ranges $313 \leqslant T \leqslant 453$ K and $0.2 \leqslant P \leqslant 7.7$ MPa. High-accuracy measurements of the speed of sound $u(T, P)$ in the mixture were made over the ranges $260 \leqslant T \leqslant 400$ K and $0.05 \leqslant P \leqslant 1.0$ MPa in an acoustic resonator. The density and ideal-gas heat capacity were deduced from the sound-speed measurements. Figure 1 illustrates the values of P and T examined by each experimental method in relation to an estimate of the dew curve.

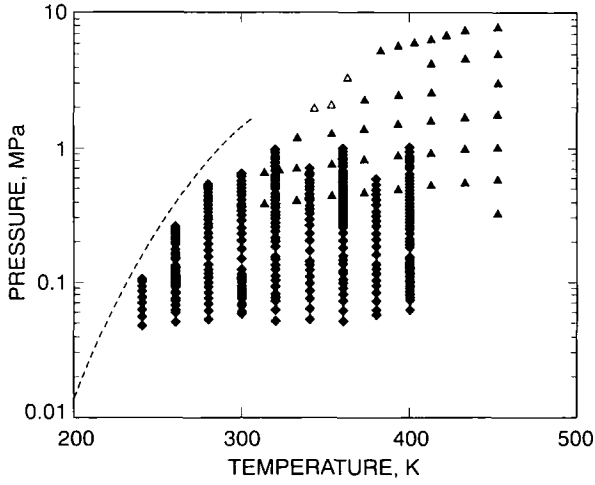

Fig. 1. The pressure-temperature space covered by each experimental technique. (◆) Speed-of-sound points; (▲) Burnett points; and (△) Burnett points left out of the fit due to their proximity to the critical point. (---) Estimate of the dew curve.

A virial equation of state with nine adjustable parameters was fit to the combined data set $\rho(P, T)$ and $u(P, T)$. The temperature dependencies of the second, third, and fourth virial coefficients were chosen to be those of hard-core square-well potentials [1]. The fifth virial coefficient was chosen to be temperature independent. The fitted equation of state reproduced the Burnett pressures or densities with a fractional RMS deviation of 0.038% (see Fig. 2) and reproduced the measured sound speeds with a fractional RMS deviation of 0.03% (see Fig. 3). The equation of state from this work was compared to another virial formulation whose coefficients were predicted from a model (see Fig. 4). The basis of the predictive model was the correlation of Pitzer and Curl [2] as modified by Tsonopoulos [3] and Weber [4–6]. In the ranges of T and P that were spanned by the speed-of-sound measurements, the gas phase densities of the mixture calculated from the predictive model differed from the experimentally deduced densities by a fractional RMS deviation of only 0.091%. In the ranges of T and P that were spanned by the Burnett/isochoric measurements, the predicted densities differed from those measured by a fractional RMS deviation of 0.254%.

The ideal-gas heat capacity of the mixture $C_p^0(T)$ was also deduced from the speed of sound measurements. The difference between $C_p^0(T)$ determined from this work and the ideal-gas heat capacity calculated from the pure species is less than 0.1% (see Fig. 5). This is consistent with the

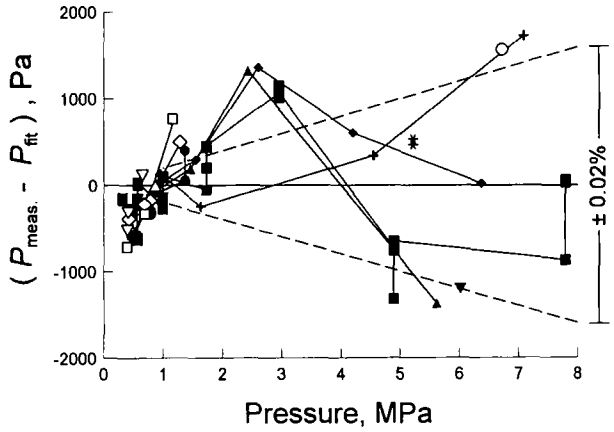

Fig. 2. Difference plot of measured Burnett pressures from those calculated from the fitted equation of state. The 0.02% deviation boundaries are indicated. (■) 453 K; (+) 433 K; (○) 423 K; (◆) 413 K; (▼) 403 K; (▲) 393 K; (*) 383 K; (●) 373 K; (★) 363 K; (◇) 353 K; (×) 343 K; (□) 333 K; (△) 323 K; (▽) 313 K.

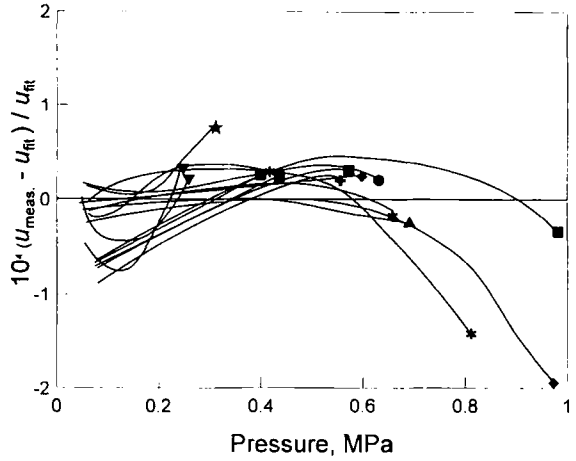

Fig. 3. Deviation plot of measured sound speed from that calculated from the fitted equation of state. (■) 400 K; (+) 380 K; (◆) 360 K; (▲) 343 K; (*) 320 K; (●) 300 K; (★) 280 K; (▼) 260 K.

careful preparation and handling of the mixture that prevented fractionation as the data were taken.

The two measurement techniques are briefly described in Section 2. The reader is directed to the indicated references for more details about these techniques. The sample preparation and analysis for impurities are

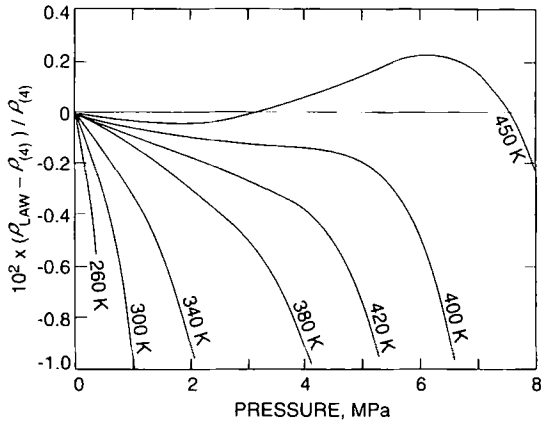

Fig. 4. Deviation plot of densities calculated from the fitted equation of state from those calculated from the predictive model of Weber [4–6], where the deviations were less than 1%.

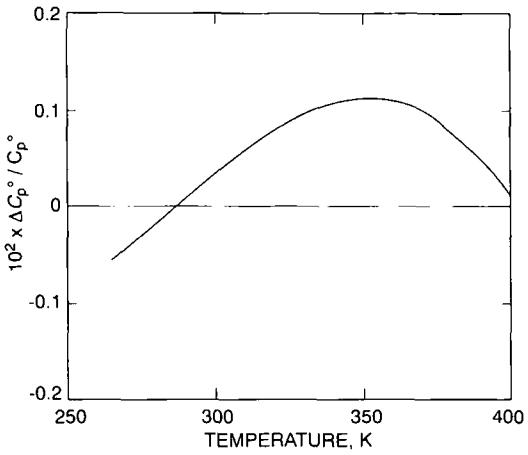

Fig. 5. Deviation plot of $C_p^0(T)$ as deduced from the sound-speed measurements against $C_p^0(T)$ calculated from the molar contributions of the pure components.

described in Section 3. The experimental results and data analysis are presented in Section 4. In Section 5 we compare these results with other sources.

2. MEASUREMENT TECHNIQUES

2.1. Burnett/Isochoric Measurements

A detailed description of the Burnett apparatus has been given elsewhere [7–9]. The heart of the apparatus consisted of two cylindrical vessels with volumes $V_1 \approx 27\ \text{cm}^3$ and $V_2 \approx 18\ \text{cm}^3$. These volumes had been bored out from opposite ends of a solid nickel cylinder. The sample volume V_1 was bounded at one end by a diaphragm that was used as a very sensitive, differential pressure transducer (DPT) [10]. The diaphragm was an integral part of V_1, and its displacement was sensed capacitively. The DPT was used to indicate when the pressure of the sample in V_1 and the pressure of argon, on the opposite side of the diaphragm, were balanced. Connected to the argon manifold were a quartz bourdon-tube pressure gauge, a deadweight piston gauge, and a pressure controller. The pressure controller maintained a null pressure difference across the diaphragm. The sample volume, expansion volume, piping, and transducer spaces were in a thermostated bath that was stable to within approximately 1 mK. Temperature measurements were made with a standard platinum resistance thermometer calibrated on ITS-90 and a high-precision DC multimeter.

Temperature and pressure measurements were performed along isochores from the highest temperature (453 K in this case) down to the coexistence curve. The highest-density isochore was measured first. After the temperature was returned to 453 K, a single Burnett expansion reduced the density in preparation for the next isochore. Measurements on several isochores were performed in this manner. The lowest-density isochore was the one for which the pressure at 453 K was approximately 250 kPa. Uncertainties in the pressure measurement made further expansions unproductive. The isochore measurements were fully automated, whereas the Burnett expansions and piston gauge operation required manual input. The isochore densities were determined from the Burnett expansions at 453 K. The cell constant, $N = 1.781327 \pm 0.000035$, had been determined from a previous calibration with helium.

Pressure measurements were made with a quartz bourdon-tube gauge calibrated against a deadweight piston gauge. The standard uncertainties associated with the measurement of pressure were given by $\mu_p = \sqrt{(50 \times 10^{-6} P)^2 + (88\ \text{Pa})^2}$. A correction was made for the thermal expansion of the sample volume V_1 such that the density on the jth isochore is related to the density on the 0th isochore at $T_0 = 273.15$ K, through

$$\rho_j(T) = \left(\frac{\rho_0}{N^j}\right)\left(1 + \int_{T_0}^{T} \alpha(T)\, dT\right) \tag{1}$$

where the thermal expansion coefficient $\alpha(T) = (37 + 0.038[T(\text{K}) - 273]) \times 10^{-6}\ \text{K}^{-1}$ as obtained from Ref. 11.

2.2. Speed-of-Sound Measurements

The speed of sound in the gaseous mixture was measured with a high-accuracy acoustic resonance technique developed by our laboratory [12, 13]. A detailed description of the apparatus and the elaborate acoustic model used to reduce the data has been given in previous publications [14, 15]. A brief summary is given here.

The speed of sound in the gaseous mixture was determined from measurements of the acoustic modes of the gas confined within a cylindrical cavity. The resonance frequencies and half-widths of several acoustic modes were determined from fits to the complex frequency response in the vicinity of each mode. The measured resonance frequencies were corrected for the effects of viscous and thermal energy losses with a well-established acoustic model [14, 16–18]. The speed of sound in the sample was determined from the corrected resonance frequencies and the dimensions of the

cylinder. The dimensions of the resonator as a function of temperature were determined from resonance measurements using argon, a gas for which the properties are accurately known.

Two electroacoustic transducers (a source and a detector) in separate enclosures were located outside of the fluid bath at ambient temperature. Sound was transmitted between the transducers and the resonator through acoustic waveguides filled with argon. Two thin metal diaphragms, mounted flush with the interior of the resonator, separated the argon from the sample gas within the resonator. The argon pressure in the waveguides and in the transducer enclosures was equal to the sample pressure in the resonator so that the stress on the diaphragms was minimum. A 13-kPa full-scale DPT was used to indicate the pressure difference between the argon and the sample gas. The argon pressure was measured with a quartz bourdon-tube pressure gauge. The pressure gauge had been calibrated with a deadweight piston gauge referenced to a calibrated barometer and was found to have a standard uncertainty of $\mu_p = \sqrt{(100 \times 10^{-6} P)^2 + (30\ \text{Pa})^2}$. The differential pressure transducer and the gas manifold were maintained near 350 K to prevent condensation of the sample at high pressures. The resonator was in a thermostatically controlled bath with millikelvin stability. A 25-Ω capsule-type standard platinum resistance thermometer and a high-precision DC multimeter were used to measure the temperature. All temperatures are reported on the ITS-90.

The speed of sound was measured on isotherms starting at the highest pressure. The highest pressure was 1 MPa or 80% of the sample's dew point, whichever was lower. The resonance frequencies at each state were measured after the temperature and pressure had stabilized. To reduce the sample pressure, a portion of the sample was removed from the resonator and collected in a cold trap at 77 K. This process was repeated down to a pressure of approximately 50 kPa, where the decrease in the signal-to-noise ratio prevented further measurements. The data acquisition and instrument control for each isotherm were fully automated; however, the sample was loaded into the resonator manually.

Our resonance technique yields sound speeds with random uncertainties of about 0.01% corresponding to two standard deviations (2μ). As discussed below, the constant-pressure ideal-gas heat capacity $C_p^0(T)$ (Table I) is obtained from the zero-pressure limit of the speed of sound with a 2μ uncertainty of about 0.1% or less. The dominant uncertainty in the technique results from our ignorance of the true gas composition and of the composition changes during the measurements. The virial equation of state is fit to the speed-of-sound surface $u(P, T)$ with the aid of exact thermodynamic expressions that relate the acoustic virial coefficients to the virial coefficients in the equation of state [1]. Our laboratory has

Table I. Parameters for Virial Coefficients and Ideal-Gas Heat Capacities

C_p^0/R	A_0	3.7603
	A_1 (K^{-1})	1.2854E−02
	A_2 (K^{-2})	2.3941E−05
	A_3 (K^{-3})	−3.4394E−08
$B(T)$, ($m^3 \cdot mol^{-1}$)	b_0 ($m^3 \cdot mol^{-1}$)	8.0848E−05
	λ	1.2746
	ε (K)	549.72
$C(T)$, ($m^3 \cdot mol^{-1}$)^2	b_0 ($m^3 \cdot mol^{-1}$)	2.2374E−04
	λ	1.1558
	ε (K)	531.60
$D(T)$, ($m^3 \cdot mol^{-1}$)^3	b_0 ($m^3 \cdot mol^{-1}$)	3.2326E−06
	λ	1.5
	ε (K)	538.27
$E(T)$, ($m^3 \cdot mol^{-1}$)^4	E_0 ($m^3 \cdot mol^{-1}$)^4	−1.6522E−16

previously used this procedure when reporting on the speed of sound in numerous refrigerants [19–23] and other fluids.

3. SAMPLE PREPARATION

The ternary mixture was prepared at NIST from very pure components by an accurate gravimetric technique. The mole fractions were 0.34607 (HFC-32), 0.30062 (HFC-125), and 0.35331 (HFC-134a). The entire sample (5.2949 mol) was stored as a gas in an 18-L container at ambient temperature. The sample was convectively mixed for several hours prior to use. The mixture was analyzed with a gas chromatograph (GC) equipped with a thermal conductivity detector. A prompt peak with a fractional area of 0.0165% was observed. This contaminant was analyzed with a mass spectrometer, which showed that it contained N_2, O_2, and H_2O in the same proportions as ambient air.

3.1. Burnett Measurements

About 3 standard L was carefully removed from the storage cylinder and condensed into a smaller stainless-steel cylinder with a volume of about 150 cm^3. This aliquot was condensed at 77 K and the remaining noncondensible gases were pumped away. The smaller cylinder was heated above the critical temperature for several hours to ensure that the sample was in a single phase and well mixed. From this heated cylinder a fraction of the sample was transferred through heated tubing to the Burnett apparatus, which itself was heated above the critical temperature of the

mixture. After the Burnett data were collected, the sample was analzed with a gas chromatograph and compared with the original sample. Air was again detected within the sample with a peak area of about 0.015% of the total. The source of this air is unknown but most likely due to less than adequate degassing. The variations in relative peak areas of the constituent components of the original sample and the sample studied were within the uncertainties of the gas chromatograph ($\approx 1\%$).

3.2. Speed-of-Sound Measurements

Sample composition is extremely important in speed-of-sound measurements. The square of the speed of sound is inversely proportional to the average molecular weight m of the sample. The ideal-gas heat capacity $C_p^0(T)$ is deduced from speed-of-sound data through the relation

$$\frac{C_p^0(T)}{R} = \lim_{p \to 0} \frac{1}{1 - RT/(mu^2)} = \frac{1}{1 - 1/\gamma^0} \tag{2}$$

Since $\gamma^0 (\equiv C_p^0/C_I^0) \approx 1.1$ for this mixture, the uncertainty in $C_p^0(T)$ is approximately nine times the uncertainty in m. When speed-of-sound measurements are performed on a gas mixture, special techniques must be employed to ensure that the sample's composition is constant.

The sample cylinder was connected to the gas handling system by a short length of $\frac{1}{16}$-in.-I.D. tubing and a needle valve. The tubing, needle valve, and manifold were heated to ~ 350 K. The flow rate was restricted by the heated needle valve to avoid phase separation while the gas expanded. The speed of sound was measured in three samples. Sample 1 was the original mixture used to prepare the Burnett sample. Sample 2 was prepared to determine the effects of the air impurity on the speed of sound. Sample 3 was prepared to extend the measurements to higher pressures.

Sample 1 was taken directly from the 18-L storage cylinder. In this way, the resonator could be loaded with a fresh aliquot of sample at the start of each isotherm. Prior to the sound-speed measurements, the mixture was never allowed to condense into the two-phase region where fractionation would occur. The maximum pressure was limited to the pressure in the storage cylinder, which was about 0.7 MPa at room temperature.

Sample 2 was taken from the storage cylinder and degassed by repeated freeze/pump/thaw cycles between 77 K and room temperature until the residual pressure above the solid at 77 K was less than 0.1 Pa. This procedure reduced the amount of air in the sample by a factor of 1000 or more. The sample was then convectively mixed for several hours.

Sample 3 was prepared to enable speed-of-sound measurements at pressures above 0.7 MPa. Aliquots of the sample from the storage container were cryopumped, in two stages, into a 1-L container. The sample was single phase at temperatures above about 320 K. This third sample was convectively mixed for several hours with a temperature gradient between 350 and 400 K along its length. Aliquots of this third sample were then loaded into the resonator while the sample bottle, gas manifold, and resonator were maintained well above 320 K. Pressures up to about 1.0 MPa were obtained with this technique.

4. RESULTS

4.1. Burnett Results

Gas-phase densities $\rho(P, T)$ were determined from measurements on six isochores and one Burnett isotherm at 453 K. Eighty-eight T, P measurements covered the ranges $313 \leqslant T \leqslant 453$ K and $0.2 \leqslant P \leqslant 7.7$ MPa. A systematic offset of 0.08% between the Burnett densities and the densities obtained from the speed of sound was attributed to a slight difference in the compositions of the mixtures measured in the two experiments. A correction, based on the speed-of-sound in Sample 2 discussed below, was applied to the Burnett data to account for the known air impurity and a shift in the relative composition due to handling. A single multiplicative factor equal to 1.0008 was used to correct the Burnett density data. The corrected results are given in Table II. Seven Burnett density measurements at the three pressure-temperature states closest to the critical point were found consistently to fall outside the 3μ uncertainty limits when simultaneously fit with the sound-speed results. These seven points were excluded from the final fit and are indicated in Fig. 1 and in Table II. Possible causes for the inability to reproduce these densities include their proximity to the critical point, limitations in the algebraic representation of the temperature dependence of the virial coefficients, or unidentified experimental uncertainties. Regardless, the statistics support the exclusion of these measurements from the final fit.

4.2. Speed-of-Sound Measurements

The speed-of-sound $u(T, P)$ in the mixture was measured for pressures between 0.05 and 1.0 MPa on 16 isotherms between 260 and 400 K. Two resonance modes (one longitudinal and one radial) were measured at each pressure. The tabulated sound speeds are an average over the two modes weighted by the standard deviation of the fits to the individual resonances.

Table II. Corrected Burnett $\rho(P, T)$ Measurements

T (K)	P (kPa)	ρ (mol · L^{-1})	T (K)	P (kPa)	ρ (mol · L^{-1})	T (K)	P (kPa)	ρ (mol · L^{-1})	T (K)	P (kPa)	ρ (mol · L^{-1})
382.74	5219.94	2.76312	453.13	2952.96	0.86817	453.11	1731.52	0.48737	453.19	997.14	0.27360
382.74	5220.01	2.76312	413.22	2609.45	0.86968	453.13	996.76	0.27360	453.17	567.75	0.15359
393.16	5615.91	2.76192	393.14	2431.73	0.87041	453.13	996.72	0.27360	453.17	567.72	0.15359
403.16	5989.30	2.76076	373.13	2250.56	0.87113	433.12	949.31	0.27384	433.14	541.29	0.15373
413.28	6362.34	2.75958	353.16	2064.34	0.87184[a]	413.14	901.31	0.27408	433.19	541.39	0.15373
413.28	6362.34	2.75958	343.11	1968.30	0.87219[a]	393.19	852.88	0.27431	413.18	515.42	0.15386
423.17	6722.37	2.75840	343.11	1967.54	0.87219[a]	373.14	803.69	0.27453	393.18	488.88	0.15399
433.12	7079.60	2.75722	343.11	1967.57	0.87219[a]	373.14	803.56	0.27453	373.15	462.29	0.15411
453.08	7785.02	2.75482	453.19	2953.33	0.86816	373.14	803.52	0.27453	373.16	462.62	0.15411
453.06	7785.43	2.75482	453.19	2953.39	0.86816	313.13	652.03	0.27519	373.16	462.57	0.15411
453.06	7785.39	2.75482	453.14	1731.41	0.48737	323.16	677.87	0.27508	353.16	435.82	0.15424
453.05	4888.65	1.54650	453.14	1731.42	0.48737	332.82	702.70	0.27498	353.16	435.82	0.15424
453.05	4888.72	1.54650	433.12	1641.96	0.48780	332.82	702.67	0.27498	333.14	408.40	0.15436
433.15	4550.02	1.54785	413.14	1552.67	0.48822	353.16	754.13	0.27476	333.14	408.40	0.15436
413.13	4201.84	1.54918	393.19	1461.64	0.48863	373.13	803.70	0.27453	313.13	381.36	0.15448
363.14	3286.97	1.55240[a]	373.14	1368.96	0.48903	373.12	803.49	0.27453	313.14	381.19	0.15448
363.14	3286.90	1.55240[a]	373.14	1368.62	0.48903	373.12	803.50	0.27453	453.07	567.15	0.15359
363.14	3286.97	1.55240[a]	373.14	1368.62	0.48903	433.07	949.24	0.27384	453.12	567.19	0.15359
453.14	4889.61	1.54650	353.16	1274.54	0.48943	433.17	949.49	0.27384	453.11	567.86	0.15359
453.15	4890.30	1.54650	333.15	1177.50	0.48982	453.10	996.56	0.27360	453.11	567.83	0.15359
453.15	4890.41	1.54650	453.12	1731.10	0.48737	453.21	996.86	0.27360	453.13	321.29	0.08623
453.13	2952.87	0.86817	453.11	1731.54	0.48737	453.19	997.16	0.27360	453.13	321.26	0.08623

[a] Points left out of fit due to proximity to the critical point.

Very small corrections were applied to the results from Samples 1 and 3 to account for composition differences, based on the results from Sample 2. The corrected sound speeds are given in Tables III, IV, and V.

The speed of sound in Sample 2 was measured on four isotherms: two at 400 K, one at 260 K, and one at 320 K. The mutually consistent results for the redundant isotherms at 400 K demonstrate that the sample was fully mixed and that the sample's composition did not change during handling. Although the maximum attainable pressure was 300 kPa, due to the limited quantity of this purified sample, the pressure range was adequate to determine the ideal-gas heat capacity. Based on the GC analysis, we assumed that the ideal-gas heat capacity deduced from Sample 2 represented the pure mixture.

Most of the acoustic measurements in this work were performed with Sample 1. The speed of sound in Sample 1 was measured on 8 isotherms between 260 and 400 K. The resonator was loaded with a fresh aliquot before each isotherm. The high degree of consistency in the speed of sound among the isotherms is a strong argument that the mixture composition was not changed by our gas handling technique. Due to the small air impurity detected in the GC analysis, the speed of sound in Sample 3 was observed to be about 140 ppm higher than the speed of sound in Sample 2. Speed of sound in Sample 1 was corrected for the air impurity based on the results from Sample 2. Since the amount of air was small, it was necessary to correct the ideal-gas speed of sound only. The acoustic virial coefficients

Table III. Corrected Speed-of-Sound Measurements in Sample 1

P (kPa)	u ($m \cdot s^{-1}$)	$\mu[u]/u$ (ppm)
	$T = 399.97$ K	
577.39	197.192	31
558.02	197.351	23
530.15	197.581	17
503.53	197.799	15
478.26	198.008	18
454.24	198.204	18
431.42	198.391	8
409.87	198.568	15
389.37	198.735	6
369.86	198.895	6
351.46	199.043	13
333.93	199.188	0

Table III. *(Continued)*

P (kPa)	u ($m \cdot s^{-1}$)	$\mu[u]/u$ (ppm)
307.78	199.400	4
282.77	199.603	10
268.87	199.715	19
243.30	199.924	10
220.81	200.105	21
200.68	200.268	25
175.30	200.471	43
153.64	200.649	29
142.22	200.740	40
131.86	200.823	44
122.33	200.901	43
112.43	200.980	54
101.17	201.071	53
91.22	201.152	53
81.34	201.230	47
72.15	201.307	34
	$T = 379.97$ K	
555.61	191.743	11
513.69	192.156	14
474.96	192.535	3
439.70	192.880	1
403.27	193.234	4
369.62	193.562	4
322.17	194.021	17
307.37	194.163	20
280.22	194.425	16
256.48	194.654	21
228.69	194.922	15
204.37	195.154	28
182.95	195.359	30
159.12	195.587	40
134.11	195.826	27
121.87	195.942	36
113.18	196.025	38
101.73	196.134	42
92.23	196.225	39
82.46	196.319	33
71.32	196.426	29
61.64	196.519	33
56.22	196.573	41

Table III. *(Continued)*

P (kPa)	u ($m \cdot s^{-1}$)	$\mu[u]/u$ (ppm)
	$T = 359.98$ K	
603.66	185.226	60
583.83	185.463	57
557.44	185.779	70
532.48	186.072	51
508.72	186.353	45
486.01	186.621	42
464.51	186.873	34
431.77	187.258	39
412.79	187.479	33
384.36	187.811	24
368.13	188.000	13
351.85	188.189	9
323.53	188.516	5
299.09	188.799	0
274.74	189.079	3
253.01	189.330	1
227.71	189.620	12
200.75	189.927	10
175.97	190.210	12
154.88	190.450	24
143.76	190.577	19
133.75	190.691	12
122.37	190.817	21
113.42	190.920	23
103.01	191.036	23
96.61	191.109	22
81.10	191.286	22
71.59	191.398	4
61.55	191.514	0
	$T = 339.98$ K	
689.59	177.470	46
661.68	177.883	33
633.77	178.295	34
606.83	178.691	30
564.66	179.305	14
540.74	179.654	22
503.77	180.187	18
482.20	180.498	16
444.30	181.040	12

Table III. *(Continued)*

P (kPa)	u (m·s^{-1})	$\mu[u]/u$ (ppm)
413.63	181.477	15
395.96	181.727	5
368.69	182.111	2
343.30	182.468	1
316.71	182.840	5
284.40	183.291	8
260.69	183.620	6
229.25	184.054	10
202.46	184.423	7
170.06	184.866	17
142.01	185.249	14
142.01	185.249	15
130.86	185.400	18
121.09	185.530	36
109.55	185.693	2
97.49	185.853	19
85.76	186.013	12
75.01	186.159	2
63.16	186.320	11
52.53	186.465	42
	$T = 319.99$ K	
659.36	170.635	87
596.12	171.804	78
558.23	172.494	69
536.33	172.889	60
515.17	173.269	57
482.03	173.861	49
451.45	174.402	37
422.82	174.906	34
406.06	175.200	33
380.40	175.645	22
353.17	176.117	17
320.00	176.687	13
297.16	177.077	14
266.66	177.595	7
239.77	178.049	3
208.14	178.578	4
181.05	179.030	1
153.00	179.495	1
143.38	179.653	2

Table III. *(Continued)*

P (kPa)	u ($m \cdot s^{-1}$)	$\mu[u]/u$ (ppm)
133.30	179.819	5
123.98	179.972	7
113.03	180.152	3
103.21	180.312	2
91.49	180.504	4
81.41	180.670	14
72.12	180.822	25
61.74	180.993	37
51.20	181.161	40
	$T = 299.99$ K	
631.94	163.059	84
610.98	163.561	73
590.74	164.041	68
559.99	164.764	56
530.87	165.440	51
494.94	166.263	47
469.45	166.839	40
438.64	167.530	34
410.05	168.164	30
381.08	168.801	28
361.80	169.221	24
336.68	169.764	18
312.28	170.286	15
285.58	170.854	13
255.88	171.480	12
229.92	172.022	8
202.65	172.586	11
176.82	173.116	11
150.12	173.660	17
123.13	174.205	7
112.59	174.418	23
106.07	174.547	11
99.17	174.686	12
92.67	174.816	18
85.46	174.960	15
79.01	175.091	37
75.79	175.154	30
67.20	175.325	36
60.37	175.462	42
57.97	175.509	40

Table III. *(Continued)*

P (kPa)	u ($m \cdot s^{-1}$)	$\mu[u]/u$ (ppm)
	$T = 280.00$ K	
308.44	163.242	79
289.40	163.762	91
269.22	164.306	67
251.17	164.789	66
231.33	165.315	61
212.05	165.820	58
192.38	166.331	48
172.67	166.839	42
153.02	167.342	38
132.77	167.856	35
122.92	168.104	31
115.53	168.289	28
107.33	168.494	27
98.94	168.705	40
91.41	168.891	35
83.22	169.095	38
75.35	169.289	31
67.91	169.475	62
60.97	169.646	65
53.65	169.824	50
	$T = 260.00$ K	
256.63	157.040	39
250.23	157.266	29
234.80	157.809	35
220.26	158.314	42
206.49	158.788	45
192.33	159.269	33
176.68	159.797	43
162.40	160.274	47
147.30	160.772	45
133.92	161.210	47
123.80	161.540	58
114.58	161.836	49
106.71	162.088	52
98.97	162.236	60
90.83	162.593	57
83.52	162.825	62
75.32	163.085	75
67.07	163.342	73
59.47	165.580	83
51.30	163.836	50

Table IV. Speed-of-Sound Measurements in Sample II

P (kPa)	u ($m \cdot s^{-1}$)	$\mu[u]/u$ (ppm)
	$T = 399.97$ K	
392.17	198.715	4
346.93	199.083	22
295.80	199.500	18
243.89	199.922	20
192.44	200.338	36
139.15	200.769	43
128.71	200.852	46
115.23	200.961	49
101.19	201.075	54
88.18	201.179	56
75.15	201.288	34
61.34	201.400	55
	$T = 399.97$ K	
437.30	198.345	6
381.84	198.799	2
323.87	199.272	8
266.40	199.737	18
205.31	200.233	24
143.90	200.729	34
128.52	200.852	45
115.21	200.960	43
100.87	201.074	50
87.87	201.179	52
74.89	201.287	42
	$T = 319.99$ K	
397.29	175.356	80
350.07	176.175	68
303.42	176.974	63
252.47	177.841	61
204.07	178.651	32
152.00	179.512	13
135.42	179.785	13
120.92	180.024	6
108.08	180.234	5
91.08	180.510	4
76.23	180.756	26
60.83	181.013	38

Table IV. *(Continued)*

P (kPa)	u ($m \cdot s^{-1}$)	$\mu[u]/u$ (ppm)
	$T = 260.00$ K	
244.83	157.458	107
226.44	158.100	93
199.40	159.026	88
175.40	159.835	76
151.40	160.633	73
126.83	161.433	64
112.27	161.901	54
102.78	162.208	51
92.43	162.536	49
82.31	162.857	63
72.08	163.179	66
61.67	163.506	71

Table V. Corrected Speed-of-Sound Measurements in Sample 3

P (kPa)	u ($m \cdot s^{-1}$)	$\mu[u]/u$ (ppm)
	$T = 400.00$ K	
982.17	193.821	7
931.07	194.251	3
931.05	194.252	0
882.68	194.660	13
837.28	195.042	35
837.28	195.041	19
793.78	195.406	27
752.56	195.749	23
713.39	196.076	31
713.40	196.076	25
676.20	196.385	23
619.35	196.856	24
587.08	197.122	18
556.52	197.375	21
510.51	197.753	9
484.05	197.972	23
438.70	198.343	14
401.79	198.646	16

Table V. *(Continued)*

P (kPa)	u ($m \cdot s^{-1}$)	$\mu[u]/u$ (ppm)
381.11	198.813	2
361.35	198.974	1
330.94	199.224	6
303.19	199.448	8
276.40	199.664	9
252.45	199.860	17
225.56	200.078	23
201.89	200.270	26
180.74	200.440	36
153.11	200.665	27
140.29	200.767	40
133.25	200.824	41
122.00	200.914	46
115.94	200.963	46
104.48	201.056	50
95.96	201.125	50
86.71	201.198	51
78.46	201.267	47
	$T = 360.01$ K	
982.15	180.583	23
943.13	181.071	42
943.15	181.071	41
900.31	181.606	57
859.22	182.116	59
819.82	182.604	75
819.81	182.604	75
782.12	183.069	90
745.82	183.513	97
711.69	183.928	100
678.69	184.328	94
647.45	184.705	99
647.43	184.701	81
617.29	185.066	89
617.27	185.066	90
588.46	185.412	84
561.16	185.734	77
534.94	186.046	64
510.00	186.343	79
486.27	186.619	60
463.57	186.890	70

Table V. *(Continued)*

P (kPa)	u ($m \cdot s^{-1}$)	$\mu[u]/u$ (ppm)
441.91	187.143	54
401.67	187.614	49
366.10	188.027	39
338.38	188.349	34
312.86	188.645	37
285.72	188.958	22
258.09	189.276	11
233.45	189.559	14
203.98	180.896	7
178.79	190.183	0
154.37	190.460	10
140.28	190.622	5
133.89	190.694	3
123.71	190.808	14
114.39	190.911	16
105.83	191.008	17
96.55	191.114	16
88.19	191.209	13
78.70	191.315	16
70.33	191.412	2
60.70	191.523	18
	$T = 320.00$ K	
812.02	167.727	131
761.48	168.704	125
714.27	169.607	150
665.65	170.516	115
605.09	171.643	149
581.86	172.068	136
560.18	172.465	125
517.14	173.239	131
482.73	173.855	124
436.59	174.671	113
404.67	175.231	102
365.98	175.903	90
330.78	176.511	76
306.77	176.920	71
282.53	177.334	64
260.55	177.703	55
235.80	178.117	40

Table V. *(Continued)*

P (kPa)	u ($m \cdot s^{-1}$)	$\mu[u]/u$ (ppm)
215.67	178.459	39
199.23	178.733	39
198.17	178.748	31
146.67	179.603	20
132.99	179.828	16
123.41	179.983	6
112.19	180.166	7
102.11	180.331	4
91.72	180.501	11
82.54	180.650	9
71.42	180.834	25
61.75	180.989	22

(see Section 5) were left unchanged. By comparison of the ideal-gas sound speeds in Samples 1 and 2 at 300 K, the mole fraction of air in Sample 1 was determined to be 0.000387. The sound speeds from the other isotherms were corrected based on this air concentration.

Sample 3 was specially prepared to extend the acoustic measurements up to 1.0 MPa. The speed of sound was measured on four isotherms: two at 400 K, one at 360 K, and one at 320 K. Again, the replicated isotherm at 400 was consistent with the original one. The GC analysis showed Sample 3 to be pure, however, the acoustic measurements indicated that a slight composition shift had occurred during the preparation. The measured sound speeds in Sample 3 were systematically about 59 ppm higher than the speed of sound in Sample 2. The speed of sound in Sample 3 was corrected based on a comparison of the 320 K isotherms from Samples 2 and 3.

5. ANALYSIS

The $\rho(P, T)$ and $u(P, T)$ data were combined and analyzed to obtain a virial expansion for the equation of state of the form

$$P = RT\rho[1 + B(T)\rho + C(T)\rho^2 + D(T)\rho^3 + E(T)\rho^4 + \cdots] \qquad (3)$$

For this work, the expansion was truncated after the coefficient $E(T)$. To calculate the speed of sound from the equation of state, we use the thermodynamic relation $u^2 = (\partial P/\partial \rho)_S$. For dilute gases we formulate an expansion

similar to Eq. (3), but for the speed of sound in terms of the pressure. The result is

$$u^2 = \left(\frac{\gamma^0(T)\,RT}{m}\right)\left(1 + \frac{\beta_a(T)}{RT}P + \frac{\gamma_a(T)}{RT}P^2 + \frac{\delta_a(T)}{RT}P^3 + \frac{\varepsilon_a(T)}{RT}P^4 + \cdots\right) \quad (4)$$

where $\gamma^0(T) = C_p^0(T)/(C_p^0(T) - R)$, R is the universal gas constant, $m = 0.09013$ kg/mol is the molar mass, and $\beta_a(T)$, $\gamma_a(T)$, $\delta_a(T)$, and $\varepsilon_a(T)$ are the second, third, fourth, and fifth acoustical virial coefficients, respectively. The ideal-gas heat capacity is determined from the zero-pressure limit of Eq. (4), and the temperature dependence is conveniently represented as

$$\frac{C_P^0}{R} = A_0 + A_1 T + A_2 T^2 + A_3 T^3 \quad (5)$$

The ideal-gas heat capacity was determined from the low-pressure sound-speed measurements alone. The fitted coefficients in Eq. (5) were then fixed for the remainder of the analysis. The coefficients are included in Table I. The difference between the measured values of C_p^0 from this work and the values calculated from the pure components is less than 0.1%, as shown in Fig. 5.

The acoustic virial coefficients are related to the virial coefficients $B(T)$, $C(T)$, $D(T)$, and $E(T)$ in Eq. (3) by [1]

$$\beta_a = 2B + 2(\gamma^0 - 1)\,B_t + [(\gamma^0 - 1)^2/\gamma^0]\,B_{tt} \quad (6a)$$

$$\gamma_a = (L - \beta_a B)/(RT) \quad (6b)$$

$$\delta_a = (M - \beta_a C - 2RT\gamma_a B)/(RT)^2 \quad (6c)$$

$$\varepsilon_a = [N + \beta_a(2BC - D) - B(RT\gamma_a B + 3(RT)^2\,\delta_a) - 2LC]/(RT)^3 \quad (6d)$$

where

$$L = \frac{(\gamma^0 - 1)}{\gamma^0}Q^2 + \frac{(2\gamma^0 + 1)}{\gamma^0}C + \frac{(\gamma^{02} - 1)}{\gamma^0}C_t + \frac{(\gamma^0 - 1)^2}{2\gamma^0}C_{tt} \quad (7)$$

$$M = \frac{(\gamma^0 - 1)^2}{\gamma^0}Q^2(2B_t + B_{tt}) + \frac{(\gamma^0 - 1)}{\gamma^0}Q\mathscr{P} + \frac{2(\gamma^0 + 1)}{\gamma^0}D + \frac{2(\gamma^0 - 1)(\gamma^0 + 2)}{3\gamma^0}D_t + \frac{(\gamma^0 - 1)^2}{3\gamma^0}D_{tt} \quad (8)$$

$$N = \frac{(\gamma^0-1)^3}{\gamma^0} Q^2(2B_t + B_{tt})^2 B_{tt} + \frac{2(\gamma^0-1)^2}{\gamma^0} Q(2B_t + B_{tt})(C + C_t)$$
$$+ \frac{(\gamma^0-1)^2}{2\gamma^0} Q[B + (6\gamma^0-5) B_t + 3(\gamma^0-1) B_{tt}](2C_t + C_{tt})$$
$$+ \frac{(\gamma^0-1)}{4\gamma^0} \mathscr{P}^2$$
$$+ \frac{2(\gamma^0-1)}{3\gamma^0} Q[3D + (2\gamma^0+1) D_t + (\gamma^0-1) D_{tt}] + \frac{(2\gamma^0+3)}{\gamma^0} E$$
$$+ \frac{(\gamma^0-1)(\gamma^0+3)}{2\gamma^0} E_t + \frac{(\gamma^0-1)^2}{4\gamma^0} E_{tt} \tag{9}$$

with $\mathscr{P} = 2C + 2\gamma^0 C_t + (\gamma^0-1) C_{tt}$, and $Q = B + (2\gamma^0-1) B_t + (\gamma^0-1) B_{tt}$. We have used the notation of Gillis and Moldover [1], where for virial coefficient A, $A_t \equiv T(dA/dT)$ and $A_{tt} \equiv T^2(d^2A/dT^2)$.

Equations (4)–(9) show that calculation of the speed of sound from the equation of state involves first and second dervatives of the virial coefficients with respect to T. We chose analytical expressions for the temperature dependencies of the virial coefficients based on a physically motivated model. Gillis and Moldover [1] have shown that the hard-core square-well potential may be used as a practical method of determining gas density from speed of sound for T/T_c between 0.7 and 1.3. The measurements in our work fall within this temperature range.

The algebraic expressions for $B(T)$, $C(T)$, and $D(T)$ in terms of the square-well potential, the temperature T, and γ^0 are given in Eqs. (10), (11), and (12). The adjustable parameters for the square-well potential are ε, the well depth in Kelvin; λ, the ratio of the width of the well to the width of the hard core (σ; cm); and the molar volume of the hard core, $b_0 = \frac{2}{3}\pi N_a \sigma^3$ in $\mathrm{cm}^3 \cdot \mathrm{mol}^{-1}$, where N_a is Avogadro's number.

$$B(T) = b_0[1 - (\lambda^3 - 1)\Delta] \tag{10}$$

where $\Delta = e^{\varepsilon/k_B T} - 1$

$$C(T) = \tfrac{1}{8} b_0^2 (5 - c_1\Delta - c_2\Delta^2 - c_3\Delta^3)$$
$$c_1 = \lambda^6 - 18\lambda^4 + 32\lambda^3 - 15$$
$$c_2 = 2\lambda^6 - 36\lambda^4 + 32\lambda^3 + 18\lambda^2 - 16 \tag{11}$$
$$c_3 = 6\lambda^6 - 18\lambda^4 + 18\lambda^2 - 6$$

for $1 \leqslant \lambda \leqslant 2$. The algebraic expression for $D(T)$ is known only for explicit values of λ. Equation (12) gives expressions that are valid for $\lambda = 1.5$ as indicated.

$$D(T) = b_0^3(0.2869 - 0.1443\Delta - 0.1844\Delta^2 - 2.920\Delta^3 + 5.766\Delta^4 - 2.197\Delta^5 - 0.09867\Delta^6), \quad \text{for} \quad \lambda = 1.5 \qquad (12)$$

The fifth virial coefficient E was defined to be a temperature-independent parameter. Equation (3) and the auxiliary Eqs. (4)–(12) were fit to the data with a modified Levenberg–Marquardt nonlinear least-squares algorithm. As usual, we used independent sets of potential parameters for each of the virial coefficients in Eqs. (10)–(12) to overcome some of the limitations of the square-well potential. Thus, the physical significance of the potential parameters is lost; however, the temperature dependencies of the virial coefficients are well behaved outside of the fitted range. Only 13 adjustable parameters were required to describe both data sets over the entire temperature and pressure ranges. The results of the fit are given in Table I. Chi-square divided by the number of degrees of freedom (434) was 4.27. The fitted equation reproduced the Burnett densities with a fractional RMS deviation of 0.038% and reproduced the sound speeds with a fractional RMS deviation of 0.003%. Deviation plots of the speed of sound measurements and Burnett/isochoric measurements from the fitted equation of state are shown in Figs. 2 and 3, respectively.

6. DISCUSSION

Burnett PVT and acoustic resonance techniques complement each other for gas-phase equation-of-state measurements. The acoustic technique is superior to the Burnett technique for pressures under 1.0 MPa. Low-pressure capabilities are necessary at low temperatures because the coexistence curve severely limits the gas-phase pressure range. The acoustic technique can also be used at temperatures far lower than the Burnett technique. Acoustic measurements do not suffer from the effects due to adsorption that plague Burnett measurements at low temperatures. Low temperature capabilities are important if the maxima in the low order virial coefficients are to be determined. By comparison, our Burnett apparatus is capable of higher pressures and higher temperatures than our existing speed of sound apparatus. At high densities, the acoustic measurements suffer from parasitic difficult-to-model coupling of the gas motion to structural vibrations of the resonator. The two techniques combine to produce an accurate equation of state over wide ranges of pressures and temperatures.

Finally, the equation of state from this work was compared to another virial formulation whose coefficients were predicted from a model (see Fig. 4). The basis of the predictive model was the correlation of Pitzer and Curl [2] as modified by Tsonopoulos [3] and by Weber [4–6]. The model uses the thermodynamic properties the pure components and experimentally determined binary mixing parameters to determine the second and third virial coefficients for the ternary mixture. Higher-order virial coefficients are not included in this model. When the ranges of T and P were restricted to those examined with the speed-of-sound measurements, then gas-phase densities of the mixture calculated from our equation of state and from the predictive model differed by a fractional RMS deviation of only 0.091%. When the ranges of T and P were restricted to those examined by the Burnett/isochoric measurements, then the densities differed by a fractional RMS deviation of 0.254%. The maximum deviation was only 3% up to 8.0 MPa. Thus, the predictive power of Weber's model is sufficient for most engineering applications in the refrigeration industry, given that the thermodynamic properties of the pure components are known.

ACKNOWLEDGMENTS

The authors thank Dr. David Morrison from ICI Chemicals and Polymers Limited for support and Dr. Joe Magee from NIST, Boulder, for preparing the original mixture.

REFERENCES

1. K. A. Gillis and M. R. Moldover, *Int. J. Thermophys.* **17**:1305 (1996).
2. K. S. Pitzer and R. F. Curl, Jr., *J. Am. Chem. Soc.* **79**:2369 (1957).
3. C. Tsonopoulos, *AIChE J.* **20**:263 (1974).
4. L. A. Weber, *Int. J. Thermophys.* **15**:461 (1994).
5. L. A. Weber and D. R. Defibaugh, *Int. J. Thermophys.* **15**:863 (1994).
6. L. A. Weber, private communication.
7. M. Waxman and J. R. Hastings, *J. Res. Natl. Bur. Stand.* **75C**:165 (1971).
8. D. Linsky, J. M. H. Levelt Sengers, and H. A. Davis, *Rev. Sci. Instrum.* **58**:817 (1987).
9. D. Linsky, J. M. H. Levelt Sengers, and J. S. Gallagher, *Fluid Phase Equil.* **36**:149 (1987).
10. M. Waxman and W. T. Chen, *J. Res. Natl. Bur. Stand.* **69C**:27 (1964).
11. D. E. Gray (ed.), *The American Institute of Physics Handbook*, 3rd ed. (McGraw-Hill, New York, 1972), pp. 4–126.
12. M. R. Moldover, M. Waxman, and M. Greenspan, *High Temp. High Press.* **11**:75 (1979).
13. M. R. Moldover, J. B. Mehl, and M. Greenspan, *J. Acoust. Soc. Am.* **79**:253 (1986).
14. K. A. Gillis, *Int. J. Thermophys.* **15**:821 (1994).
15. K. A. Gillis, A. R. H. Goodwin, and M. R. Moldover, *Rev. Sci. Instrum.* **62**:2213 (1991).
16. A. R. H. Goodwin and M. R. Moldover, *J. Chem. Phys.* **95**:5230 (1991).
17. A. R. H. Goodwin and M. R. Moldover, *J. Chem. Phys.* **95**:5236 (1991).

18. K. A. Gillis and M. R. Moldover, *Proc. Ninth Symp. Energy Eng. Sci.* (Argonne National Laboratory, May 13–15, 1991), p. 310.
19. A. R. H. Goodwin and M. R. Moldover, *J. Chem. Phys.* **93**:2741 (1990).
20. J. J. Hurly, J. W. Schmidt, S. J. Boyes, and M. R. Moldover, *Int. J. Thermophys.* **18**:137 (1997).
21. J. J. Hurly, J. W. Schmidt, and K. A. Gillis, *Int. J. Thermophys.*, in press.
22. D. Defibaugh, K. A. Gillis, M. R. Moldover, G. Morrison, and J. W. Schmidt, *Fluid Phase Equil.* **81**:285 (1992).
23. K. A. Gillis, *Int. J. Thermophys.* **18**:73 (1997).